To appear in *Advanced Robotics*
Vol. 00, No. 00, January 2013, 1–13

Spine as an Engine: Effect of Spine Morphology on Spine-Driven Quadruped Locomotion

Qian Zhao[a*], Hidenobu Sumioka[b], Kohei Nakajima[a c], Xiaoxiang Yu[c], and Rolf Pfeifer[a]

[a]*Department of Informatics, University of Zurich, 8050 Zurich, Switzerland*; [b]*Advanced telecommunications research institute international,Japan*; [c]*Bio-Inspired Robotics Lab, Swiss Federal Institute of Technology Zurich, 8092 Zurich, Switzerland*

(*v1.0 released January 2013*)

In quadruped animals, spinal movements contribute to locomotion in terms of controlling body posture and integrating limb and trunk actions. In this paper, we develop quadruped models with different numbers of spinal joints to demonstrate the spine-driven locomotion. Actuated spinal joint(s) are exclusively employed to these models with a minimalistic control strategy. We choose some typical individuals from two models and analyze them on gait properties. Results show that employing the spine morphology with two joints can greatly enhance the stability and speed of locomotion by readjusting center of mass, increasing the stride length, and generating double flight phases similar to running cheetahs gait, which makes significant difference in the speed and the gait. Furthermore, we explore and compare models with more spinal joints. Results show that all gaits emerged from them can be categorized into three types (bounding, bounding with double flight phase, and stotting gaits). Overall, bounding gait with double flight phases is a more biologically inspired locomotive behavior; model with two spinal joints could be sufficient to emulate biological spine-driven locomotive behaviors.

Keywords: spinal engine; spine-driven locomotion; spine morphology; embodiment

1. Introduction

Over the past decades, it has been widely accepted that locomotion is generally achieved by the coordination of legs and the spine is only considered to be carried along in a more or less passive way [1]. This popular hypothesis has been accepted by most of robotics researchers as well as biologists. A considerable amount of research has been conducted on legged robots with little consideration on their spines. Most of the existing quadruped robots are very similar in their morphology, and feature a single rigid body with four legs with individually actuated hips and/or knees [2, 3]. They can perform well in some terrains, but they need precise calculation at every time step and therefore lead to high computational load. Furthermore, the resulting locomotive behavior is still much more constrained than its natural counterpart in terms of speed, energy efficiency, maneuverability, and adaptivity to rough terrain.

If we look back to the nature, we find that one of the major differences between these robots and animals is the spine. Such a spine is central to control body posture, provide the foundation to produce the leg's movement, and integrate limb and trunk actions [4]. From the evolutionary point of view, it is natural to consider the spine as an propulsive engine of the vertebrate body to maintain a central role in locomotion in all craniates. Based on mathematical simulations and analysis, Gracovetsky has proposed an alternative biological hypotheses called "Spinal Engine", which emphasizes the role of the spine in human locomotion, i.e., locomotion is firstly achieved by the motion of the spine; the limbs came after, as an improvement but not a substitute [5].

*Corresponding author. Email: zhao@ifi.uzh.ch

Then, he extended this hypothesis to quadruped animals featuring flexion-extension spinal movement [6], [7]. All of them imply that the spine is crucial to locomotion and such a spine might plays a dominant role in locomotion.

Recently, some researchers have come to realize the important role the spine plays in locomotion, but most only focused on the controller of the spinal joint, and barely paid attention to its morphology [8, 9]. All the aforementioned studies simply introduced a spinal joint connecting the fore and rear part without studying further on its morphological parameters and anatomical structure. The concept of embodiment suggests that a system's behavior is generated through the interaction between controller, body (morphology) and environment [10]. In this context, morphology should be regarded as one of important priorities to be studied. So far there are some studies with the focus on the spine morphology. For example, a biologically inspired spine has been developed and applied to a quadruped robot named Kitty to study the effect of the shape of the spinal column on locomotion [11]. Additionally, the position of the spinal joint is also studied in Kitty robot [12]. A musculoskeletal quadruped robot has been developed to investigate the stability of locomotion by changing the stiffness at the trunk in crawl, trot, and pace patterns [13]. However, if we look back to the anatomical structure of a biological spine, we find that there still exists a lot of room to study spinal morphological parameters on locomotion, in addition to the features discussed above, to gain a deep understanding of the locomotive function of the spine and how such a function is affected by morphology.

This paper focuses on investigating the role of the spine and the effect of the number of spinal joints in locomotion. First we introduce two models differing in the number of spinal joints to demonstrate the spine-driven locomotive behavior. One model has one spinal lumbosacral joint and the other one has lumbosacral joint and thoracic joint together. Second, four typical individuals from these two spinal morphologies are selected and compared regarding the gait, the attack angle, and the movement of the center of mass (CoM). The simulation results show that locomotion can be greatly enhanced by employing the second model with two joints in terms of the stability and speed. Furthermore, the effect of multiple spinal joints on spine-driven locomotion is investigated. The spine morphology varies from three spinal joints to twelve spinal joints. Each morphology is analyzed in detail in terms of gait, speed, and success ratio. Results show two spinal joints might be a feasible model to emulate the biological spine-driven locomotive behaviors.

2. Design

In this section, we describe the design of the models and spinal morphologies. Next, the selection of the morphological parameters and the design of controller are presented.

2.1 *robot design*

In this model, the fore and rear legs are fixed to the ends of the spine and have no relative rotation with respect to it. In other words, the robot is only actuated by the spine, and leg actuation is not taken into account. Our aim is to test whether or not the spine is the main power to drive the robot, inspired by the biological concept "Spinal Engine" [7], so this design is straightforward to study the function of the spine and the effect of spine morphology on locomotion.

2.2 *Spinal morphology design*

A biological spine is made up of small bones, known as vertebrae, that are stacked on top of each other to create the spinal column. The number of vertebrae varies with the species of the animals from ten in frogs to fifty six in tigers. All of the spinal movements are distributed over

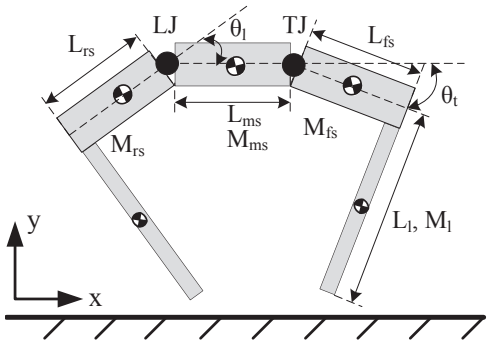

Figure 1. Planar quadruped model of $M2$. Black solid dots stand for the actuated spinal joints.

Table 1. Morphological parameters for $M2$

Parameter	L_l	L_{rs}	L_{ms}	L_{fs}	M_l	M_{rs}	M_{ms}	M_{fs}
Value	0.83 m	0.33 m	0.33 m	0.33 m	5 kg	6.7 kg	6.7 kg	6.7kg

L: length; M: weight.

l: leg; rs: rear spinal segment; ms: middle spinal segment; fs: fore spinal segment.

the connecting joints of these vertebrae.

We know that the spinal column consists of lumbosacral spine, thoracic spine, and cervical spine [7]. Hence we employed a spinal joint with one degree of freedom (DoF) to emulate the movement of each part. Because the head's movement has less effect on locomotion, we ignored cervical spine in this study. We utilized a lumbosacral joint (LJ) to mimic the role of lumbosacral spine in locomotion. Similarly, the thoracic joint (TJ) is taken to emulate the function of thoracic spine.

As a starting point, we only applied LJ into the model to study the role of lumbosacral spine, because biological findings suggest that the rear position of LJ can produce a particularly marked sagittal displacement of the pelvis [14] [15], which could plays a main role in locomotion. We name this model with LJ as $M1$. $M1$ consists of three segments which are a pair of stick-shaped legs, and a spine with a LJ.

Because of the existence of a small amount of flexion-extension movement in thoracic spine [16], we added a TJ in the middle between the shoulder and the LJ (Fig. 1) to investigate how it affects locomotion, along with lumbosacral spine. The model with these two joints is named as $M2$. If we fix the movement of TJ, which is θ_t in Fig. 1, and keep the rest parameters of $M2$, then $M2$ becomes $M1$.

We copied some of cheetah's morphological parameters (weights and sizes of the body and legs), and applied to the models, because a cheetah exhibits noticeable spinal flexion and extension movement when running [17]. Table 1 details morphological parameters chosen for $M2$.

2.3 *Controller design*

2.3.1 Minimalistic control strategy

To focus on the study of spine-driven locomotion and the effect of spine morphology on locomotion, we employed a minimalistic control strategy to this model, in which the angular position of the spinal joints is determined by the sinusoidal curve as follows:

$$\theta_l(t) = A_l \sin(2\pi f_l t) + \psi_l \tag{1}$$

$$\theta_t(t) = A_t \sin(2\pi f_t t + \phi_t) + \psi_t \tag{2}$$

where θ_l and θ_t indicate the target angular positions of the motors controlling LJ and TJ,

respectively. A, f and ψ designate the amplitude, the frequency, and the offset. The phase ϕ is the delay between the LJ and TJ. The subscript l and t denote LJ and TJ, respectively. The parameters used in the following experiments are heuristically determined as follows: $f_t = f_l = 1.5\ Hz$, $A_l \in [0°, 60°]$, and $\psi_l \in [-15°, 15°]$. The rest control parameters (A_t, ψ_t, ϕ_t) will be optimized with Genetic algorithm (GA) described in the following part. Time step t in this paper represents one actuation loop of the control program.

2.3.2 Genetic algorithm for the sinusoid function controller

GA [18] is employed to optimize the control parameters (A_t, ψ_t, ϕ_t) for TJ with the attempt to achieve fast and stable locomotive behaviors. The boundaries of these three parameters are decided as follows: $A_t \in [0°, 60°]$, $\psi_t \in [-15°, 15°]$, and $\phi_t \in [-180°, 180°]$. They are encoded as three 8 bit genes and concatenated as a chromosome. Afterwards, a cost function generates an output (the speed of the robot) from this chromosome (control parameters of the robot). Here the cost function is an experiment by which the performance of the robot is evaluated. If the robot is able to move stably and fast, then it is considered as a sucess and the speed is recorded, otherwise, the speed is 0. We set population size to 600 and the generation number to 10.

The GA starts with a group of chromosomes known as the population. Natural selection occurs each generation or iteration of the algorithm. After each generation, only the fastest 50% of the individuals are selected to continue, while the rest are deleted. The next step is to generate a second population of solutions from those selected through genetic operators: crossover and mutation. After the mutations and crossovers take place, the costs (speed) associated with the offspring and mutated chromosomes are calculated. Generation continues to evolve until iteration number exceeds 10.

3. Experimental Setup

3.1 *Simulation Setup*

We have implemented models in Mathworks matlab 2009, together with the SimMechanics toolbox, which provides a multibody simulation environment. We use blocks provided by SimMechanics to represent bodies, joints, constraints, and actuators. When the model is established, SimMechanics formulates and solves the equations of motion for the complete mechanical system automatically. In this study, motion mode of joint actuation is chosen in which only position, velocity, and acceleration of the angular joints are needed, because we mainly focus on the kinematics of the spine and its resultant locomotive behavior.

3.2 *Experimental criterion*

Locomotive behaviors of the planer quadruped model can be categorized into four types: the robot exhibits a stable rapid locomotion; it runs slowly; it exhibits unstable behavior; or it falls over or flies away. Only the first case is considered as meaningful behavior, while the rest are failures. In this paper, we use two methods together to judge the system's stabilizing behavior. Step-to-fall method is used in a way such that the robot is expected not to fall within given time or cycles. Here, we set the time to 50 s. The second one is to calculate the difference between two apex heights of CoM in every two subsequent cycles. If such a difference is less than a threshold, then we assume that this individual is stable, and the speed is recorded. Otherwise, this individual is considered to be a failure and the speed is 0. This method is simple, but it is efficient to predict the tendency of the stability. For example, if the error between the current cycle and previous cycle exceeds the threshold, but the robot is still able to move, then it suggests a rather high possibility of instable situation for the next cycle where the robot either falls over or flies away.

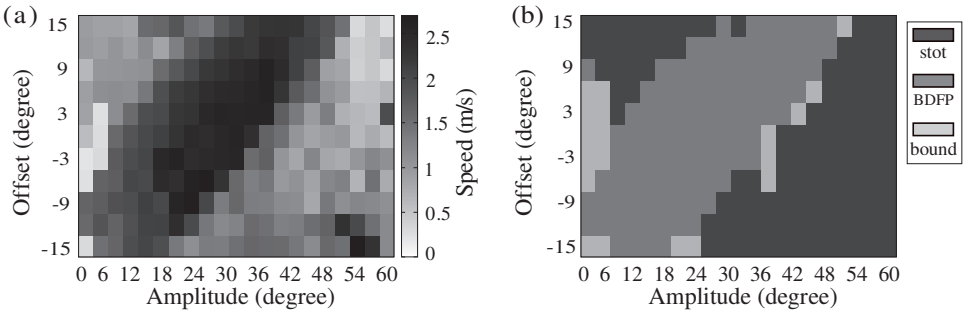

Figure 2. Speed (a) and gait categorization (b) of $M2$. X axis is amplitude (A_l), and y axis denotes offset (ψ_l) for the LJ.

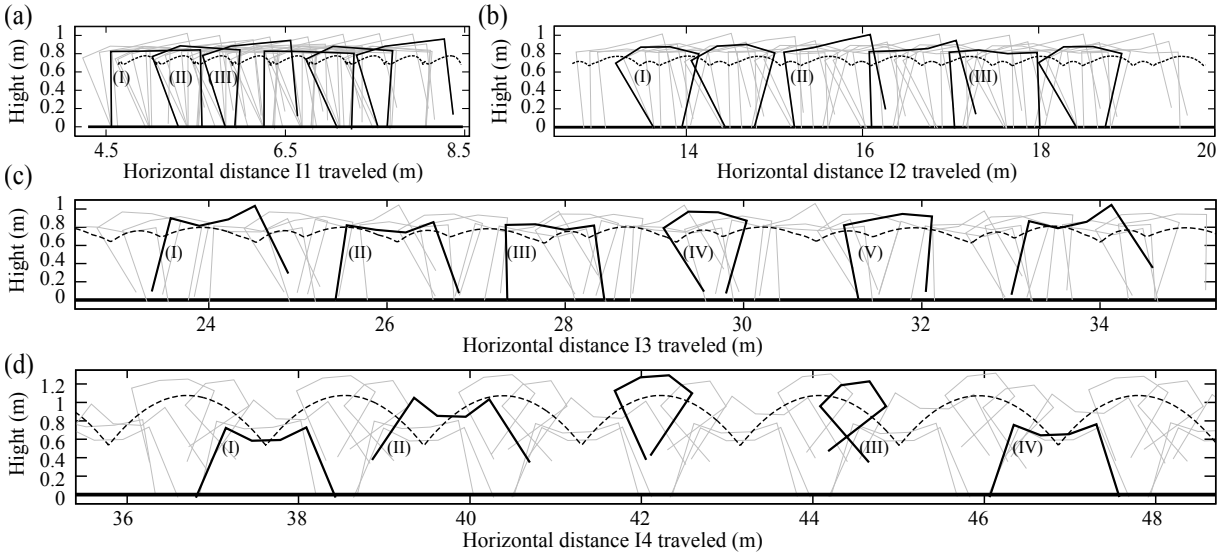

Figure 3. Stick figures illustrating three different behaviors in simulation. The body postures are illustrated every 105 and 735 (105×7) simulation steps (a), and every 105 and 630 (105×6) simulation steps (b), (c), (d) (gray and black stick figures, respectively). Dotted line represents the trajectories of absolute CoM. (a) $I1$ ($A_l = 18°$, $\psi_l = -12°$). (b) $I2$ ($A_l = 36°$, $\psi_l = -3°$). (c) $I3$ ($A_l = 30°$, $\psi_l = -3°$). (d) $I4$ ($A_l = 54°$, $\psi_l = -15°$)

4. Results

In this section, results of the overall exploration based on two proposed simplified models are presented first, followed by individual analysis in terms of CoM, attack angle, and the gait. Next, the effect of multiple spinal joints ranging from three to twelve on spine-driven locomotion is investigated. Each morphology is analyzed in terms of success ratio, speed, and gait.

4.1 *Overall exploration based on two spinal morphologies*

To achieve comprehensive behavioral analysis, we investigated the influence of amplitude (A_l) and offset (ψ_l) on the locomotive behavior for $M1$ and $M2$. We varied A_l from 0° to 60°, and ψ_l from −15° to 15° with the increment of 3° in $M1$. Then we keep the same control parameters for the LJ and optimize the rest three (A_t, ψ_t, ϕ_t) for the TJ in $M2$.

Figure 2(a) and Figure 4(a) demonstrate that locomotion is able to be generated by the spinal flexion and extension in $M2$ and $M1$. Figure 2(b) shows that there exist three gaits in $M2$: bounding (Fig. 3(b)), bounding with double flight phases (BDFP) (Fig. 3(c)) and stotting gaits (Fig. 3(d)), while $M1$ is only able to generate bounding gait (Fig. 3(a)). The fastest individuals of each gait of $M1$ and $M2$ are selected; they are named as $I1$ in $M1$, $I2$ in bounding in $M2$, $I3$ in BDFP in $M2$, and $I4$ in stotting in $M2$, respectively. Since stotting gait exhibits different locomotion pattern where all of the legs touch and leave the ground at the same time, we excluded this gait in the following analysis and will explain it later in section 4.4. Figure 4 shows that $M2$

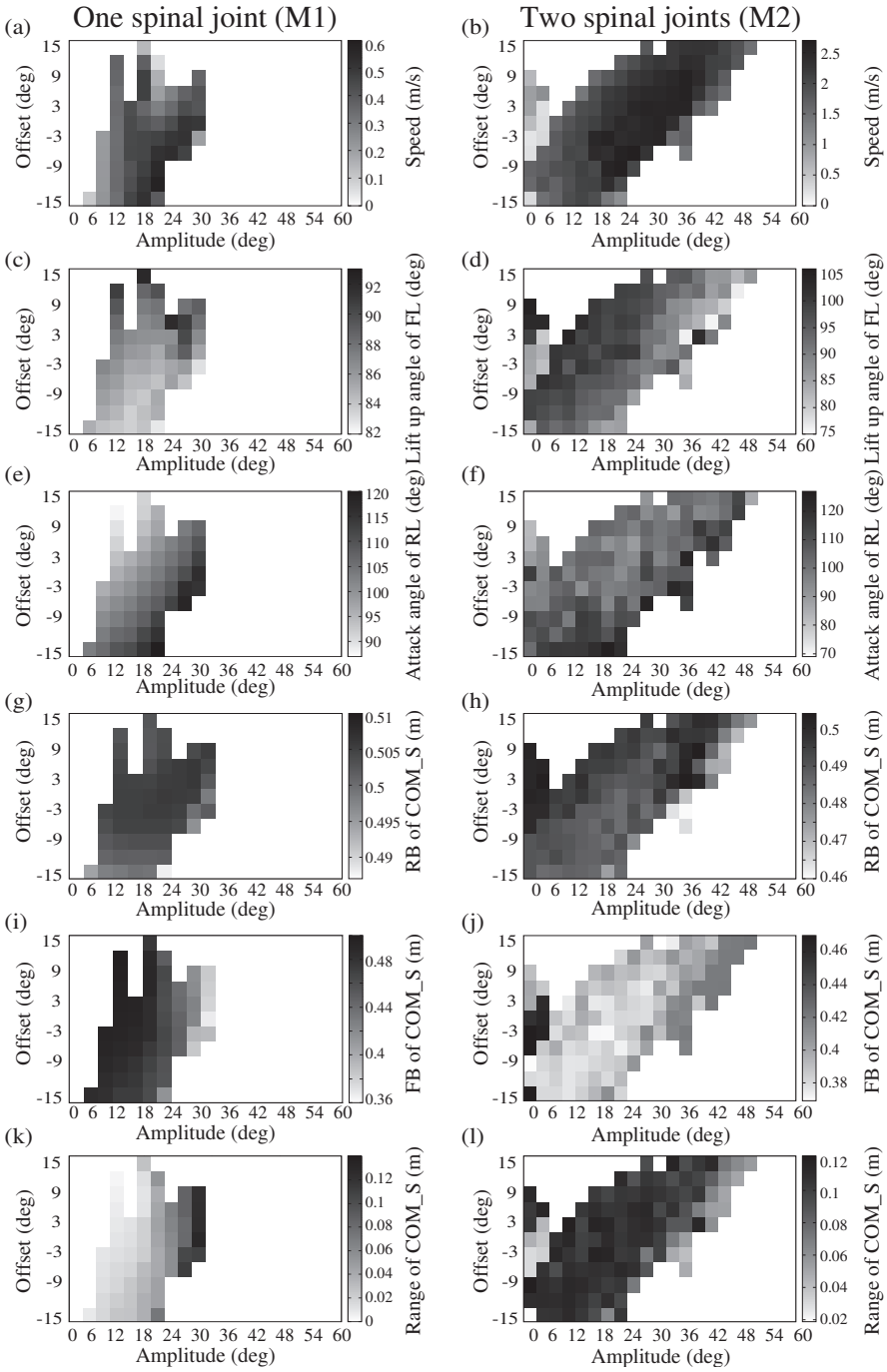

Figure 4. Comparison results of two spinal morphologies ($M1$ in the left column and $M2$ in the right). X axis is amplitude (A_l), and y axis denotes offset (ψ_l) for the LJ. The intensity of each cell represents the speed in (a), (b); the lift up angle of rear legs (RL) in (c), (d); attack angle of fore legs (FL) in (e), (f); the rear boundary (RB) of CoM_S in (g), (h); the fore boundary (FB) of CoM_S in (i), (j); the range of CoM_S in (k), (l).

can move much faster than $M1$, and its fastest performance attains 2.6 m/s, while the fastest one from $M1$ is 0.59 m/s.

The attack angle is defined as the angle formed between the leg and the ground in the forward direction when the feet touch on the ground. In both morphologies, greater attack angle of rear legs (Fig. 4(e), (f)) corresponds to faster speed (Fig. 4(a), (b)). With a larger attack angle, the rear legs can rotate the robot's body around the contact point and push it more forward. In addition, less lift up angle of fore legs (Fig. 4(c), (d)), which benefits to propel the body forward, correlates to faster speed (Fig. 4(a), (b)).

In the biological perspective, the CoM moves forward and backward alternatively with respect

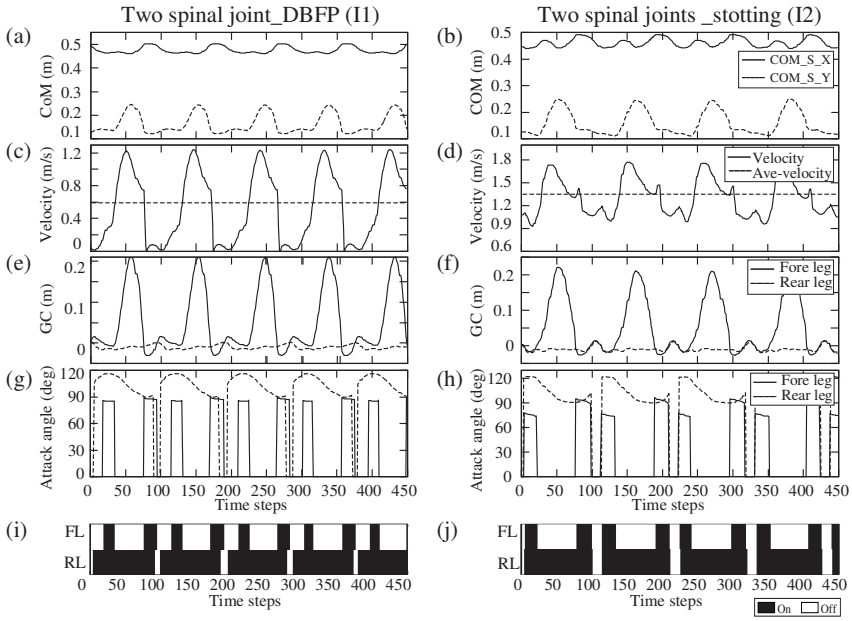

Figure 5. The left and right column are the results of $I1$, $I2$. The x axis represents time steps. From top to bottom, the y axis stands for the movement of CoM relative to the shoulder (a),(b), the velocity (c), (d), the height of ground clearance (e), (f), the attack angle (g), (h), and the footfall pattern (i), (j).

Table 2. Parameters for $I1$, $I2$ and $I3$

Parameters	A_l	ψ_l	A_t	ψ_t	ϕ_t
$I1$	18°	−12°	/	/	/
$I2$	36°	−3°	19°	13°	-0.67
$I3$	30°	−3°	24°	13°	-0.214

to its nose during locomotion [19]. Hence, we defined the CoM_S as the distance between the position of CoM and the position of the robot's shoulder, instead of the nose. The range of the CoM_S gets wider, as a result of the increasing amplitude of the bending and extension movement (Fig. 4(e), (f)). Wider range of the CoM_S (Fig. 4(k), (l)) is associated with better performance (Fig. 4(a), (b)), because it offers more freedom to adjust the CoM, benefiting the stabilization of the posture and the enhancement of the speed. Furthermore, with the increase of the speed in $M1$ and $M2$ (Fig. 4(a), (b)), the values of the rear and fore boundaries of the CoM_S get smaller (Fig. 4(g)-(j)), which suggests that the horizontal excursion of the CoM moves further to the anterior trunk region.

4.2 *Basic effects of thoracic joint*

To understand the basic effect of LJ in bounding gait and how TJ benefits to the bounding gait, along with LJ, $I1$ and $I2$ are chosen and analyzed in detail. The average speed of $I1$ is 0.59 m/s (Fig. 5(c)), while $I2$ is 1.25 m/s (Fig. 5(d)). Parameters obtained from GA described previously are given in Table 2.

4.2.1 Analysis on spine-driven locomotion

Figure 3(a), (b) show that the stable locomotive behavior of $I1$ and $I2$ can be achieved, even if leg actuation is not taken into account. We observed three prominent phases in $I1$ (Fig. 3(a)). Starting from the original posture (phase I), the spine is flexed and the rear legs are pulled forward until the maximum (phase II). This moves the CoM forward. Afterwards, the spine is extended to allow the lift up of the fore legs, leading to the back-moving of the CoM (phase III). In the next step, the fore legs touch the ground, and the CoM moves forward again (back to phase I). The same process repeats.

Table 3. Results of CoM_S in $I1$, $I2$, $I3$

	CoM_$S_{horizontal}$ (m)			CoM_$S_{vertical}$ (m)		
	Fore_b	Rear_b	Range	Low_b	High_b	Range
$I1$	0.46	0.5	0.04	0.12	0.25	0.13
$I2$	0.45	0.49	0.04	0.12	0.25	0.13
$I3$	0.39	0.49	0.1	0.11	0.29	0.18

Similarly as $I1$, $I2$ also has three important phases (Fig. 3(b)). The difference with $I1$ comes from the further flexed spine caused by combining the flexion of LJ and TJ. This then pulls the rear legs more forward than $I1$ (phase I) and leads to a higher attack angle of 123° (Fig. 5(h)), compared to $I1$ with 116° (Fig. 5(g)). The rest of the cycle follows the same procedure as in $I1$. We categorized $I1$ and $I2$ to the bounding gait due to their similar phases and footfall patterns (Fig. 3(a), (b), Fig. 5(i), (j)).

4.2.2 Attack angle

In these two models, attack angle changes along with the body posture controlled by the spinal controller. Wider range of attack angle of fore legs in $I2$ enhances locomotion, because it is able to increase the stride length by propelling the body forward further. It varies from 94° to 74° in phase I (Fig. 5(h)), as a result of the additional flexion of TJ. Therefore, it can push the body forward further than $I1$, whose angle is almost constant, 90° (Fig. 5(g)). In addition, larger attack angle of rear legs contributes to the increase of the stride length by pushing the body more forward.

4.2.3 Movement of the center of mass

Figure 5(a), (b) show that the horizontal motion of the CoM is only determined by flexion and extension of the spine. This underlines the determinant role of the spine as the main engine for the locomotion. The movement of CoM relative to the shoulder is not constant (Fig. 5(a), (b)). The horizontal excursion of the CoM is in coupling with the motion of the spine. During spinal extension, the CoM moves to the posterior part of the spine, but it moves to the anterior part during spinal flexion. The extension phase of the spine is coupled with a upward movement of the CoM. In the flexion phase, after initial ascent, the CoM moves downward (Fig. 5(a), (b)). The excursion of the horizontal and vertical movement of the CoM is shown in Table 3.

4.3 *Dynamic locomotion induced by double flight phases*

$I3$ is analyzed to investigate how BDFP gait is generated and how it contributes to the locomotion. $I3$ can reach up to 2.75 m/s (Fig. 6(c)).

4.3.1 Analysis on spine-driven locomotion

There exists a high level of coordination between spinal flexion and the placing of the feet on the ground to maximize stride length and increase speed in $I3$. $I3$ mainly differs from $I1$ and $I2$ in the gait (Fig. 3(a), (b), (c)). It is characterized by five phases, two of which are flight phases, instead of one, in each stride. Figure 3(c) shows that one takes place when the spine is at maximal extension (phase I); the other one occurs when the maximal flexion of the spine is achieved (phase IV).

However, $I3$ exhibits an unnecessary stance phase (phase III in Fig. 3(c)), which does not exist in cheetah running. We could eliminate this phase by adding actuated shoulder joints (Fig. 7). If actuated shoulder joints are employed in the very beginning of this phase to swing the fore legs backward, then the fore legs might be lifted up. In this case, the double stance phase becomes rear leg stance, and therefore $I3$ can exhibit a more cheetah-like bounding gait.

The frequency of $I3$ is the same as $I2$ and $I1$, but the speed is much faster than both, due to longer stride length. This is caused by the double flight phases exclusively showing up in $I3$.

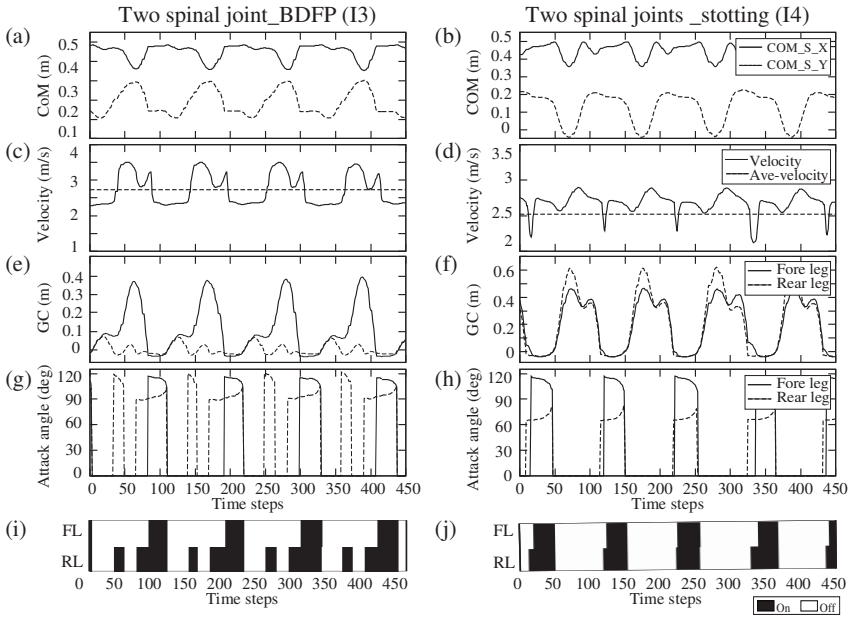

Figure 6. The left and right column are the results of $I3$, $I4$. The x axis represents time steps. From top to bottom, the y axis stands for the movement of CoM relative to the shoulder (a),(b), the velocity (c), (d), the height of ground clearance (e), (f), the attack angle (g), (h), and the footfall pattern (i), (j).

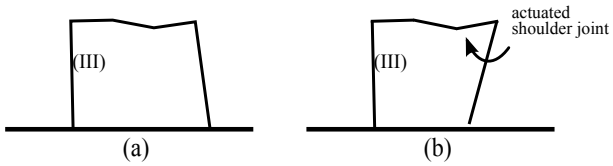

Figure 7. (a) Double stance phase (phase III) in Figure 3, and (b) the possible way to transfer (a) to rear leg stance phase by employing actuated shoulder joints.

4.3.2 Attack angle

For the rear legs, it has similar value of attack angle to $I2$, but it has a smaller lift up angle of 90° (Fig. 6(g)), which can crouch more and push the body forward further, compared to $I2$ with the angle of 105° (Fig. 5(h)).

4.3.3 Movement of the center of mass

Figure 6(a) shows that $I3$ has much wider horizontal and vertical movements of the CoM, compared to $I1$ and $I2$ during one cycle (Fig. 5(a), (b)). Table 3 shows the boundaries and the range of the CoM_S in horizontal and vertical direction. This horizontal excursion equals around 10% and vertical excursion is about 18% of the body length in $I3$. We observed that values of fore boundary and rear boundary of the horizontal movement of CoM_S in $I2$ and $I3$ are smaller than $I1$, which suggests that $I2$ and $I3$ are able to move the CoM forward more efficiently than $I1$, benefiting the rapid locomotion. Moreover, the excursion range of the CoM_S in $I3$ is wider than $I1$ and $I2$, offering more freedom to adjust the CoM to stabilize the robot itself.

4.4 *Stotting gait emerged from pronounced spinal flexion and extension movements*

Interestingly, we found stotting gait,in addition to bounding and $BDFP$ gaits in $M2$, (Fig. 3(d)). Figure 2 implies that scotting gait has more chance to take place in the high amplitude area where spine exhibits pronounced flexion and extension movements.

To understand how the stotting gait behaves, and how it differs with the other two gaits, $I4$, the fastest case is chosen and its locomotive features are analyzed. The average speed of $I4$ is

Table 4. Range of parameters for multiple spinal joints.

Morphology	Amplitude	Morphology	Amplitude	Morphology	Amplitude	Morphology	Amplitude
$M1$	$[0° : 60°]$	$M4$	$[0° : 40°]$	$M7$	$[0° : 30°]$	$M10$	$[0° : 30°]$
$M2$	$[0° : 60°]$	$M5$	$[0° : 40°]$	$M8$	$[0° : 30°]$	$M11$	$[0° : 30°]$
$M3$	$[0° : 60°]$	$M6$	$[0° : 30°]$	$M9$	$[0° : 30°]$	$M12$	$[0° : 30°]$

Note: $\psi \in [-15°, 15°]$, $\phi \in [-180°, 180°]$, the same as $M2$

2.5 m/s (Fig. 6(d)). Its four legs jump off and on the ground at the same time (Fig. 6(f), (j)).

We observed that there are four prominent phases in one cycle (Fig. 3(d)). Starting from the original posture (phase I), the robot jumps off the ground when the spine starts to flex (phase II). Then it achieves maximal spinal flexion in the air (phase III), which is immediately followed by spinal extension while the robot is still in the air (phase IV). The spine continues to extend until it lands the ground (back to phase I). In this stotting gait, there exists only one flight phase per cycle where the spinal flexion and extension take place.

4.5 *Exploration on multiple spinal joints*

To check if this simplified model with two spinal joints ($M2$) discussed previously is sufficent to emulate biological spine-driven locomotion, we extend experiments by introducing more spinal joints, while keeping most of the setting the same.

4.5.1 Experiments setting

Multiple spinal joints are employed and a new model is constructed (Fig. 8), where the number of spinal joints increases from three to twelve. We name each spine morphology by Mi, where i represents the number of spinal joints. These joints are evenly distritbuted along the spine. The total weight of the spine including all of spine segments and joints is the same as $M1$ and $M2$. We start to set the amplitude to $60°$ for each morphology. If no successful individuals can be found within the given number of 80,000, then the amplitude decreases by $10°$ until successful cases occur. In the end, the range of the parameters of each morphology is shown in Table 4. Moreover, the choice of those ranges is reasonable, because they are wider than the biological spinal motion range, e.g., cat [20], equine [21], pika [22].

4.5.2 Exploration on more spinal joints

We calculated the success ratio of each morphology by dividing the number of successful individuals which are able to move forward periodically and stably without falling over by the total number of individuals (80,000). We observed that with the increase of the spinal joints, the success ratio drops exponentially (solid black line in Fig. 9). This is caused by the increase of dimension of controller parameters, e.g., 23 parameters for $M8$. Therefore, we stopped adding spinal joints when its success ratio is below the threshold (1%). As a result, M12 is the model with the maximal number of spinal joints.

Figure 10 shows the overall exploration of the number of spinal joints ranging from one to twelve. Interestingly, we found that all of the successful individuals from randomly chosen 80,000 individuals can be categorized into three types: bounding gait, $BDFP$ gait, and stotting gait, which is the same as $M2$. Generally speaking, $BDFP$ gait outperforms the other two gaits regarding speed over all spine morphologies. $BDFP$ gait emerges when the number of spinal joints is great than one, and its average speed and maximal speed keep similar with the increase of the spinal joints. This suggests that $BDFP$ gait is caused by multiple spinal joints. However, the introduction of more than two spinal joints does not contribute too much to the speed of the robot. This implies that $M2$ is sufficient to generate fast $BDFP$ gait. Stotting gait emerges in the same spine morphologies as $BDFP$ gait. However, the fastest speed of stotting gait increased greatly from $M9$ to $M12$, while its average speed and standard deviation do not vary much. The performance of bounding gait is greatly improved when $M2$ is taken, and then it remains.

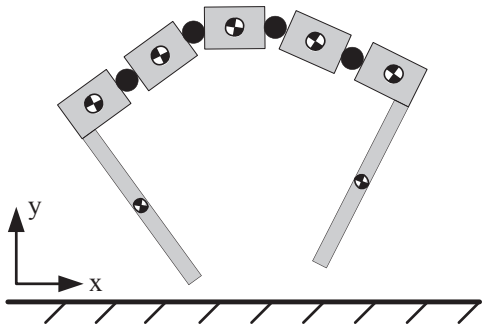

Figure 8. An example of planar quadruped model with multiple spinal joints: $M4$. Black solid dots represent the actuated spinal joints.

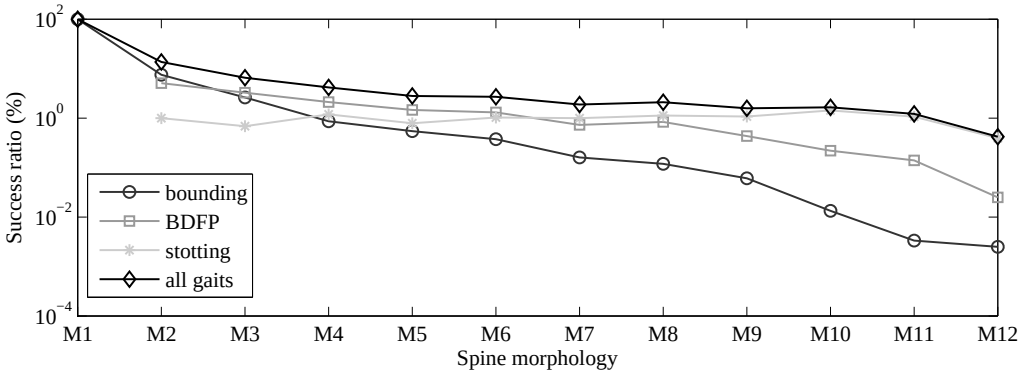

Figure 9. Success ratio of all morphologies changing from one spinal joint to twelve. X axis stands for the spine morphology ranging from one to twelve spinal joints. Note that y axis is in logarithmic scale.

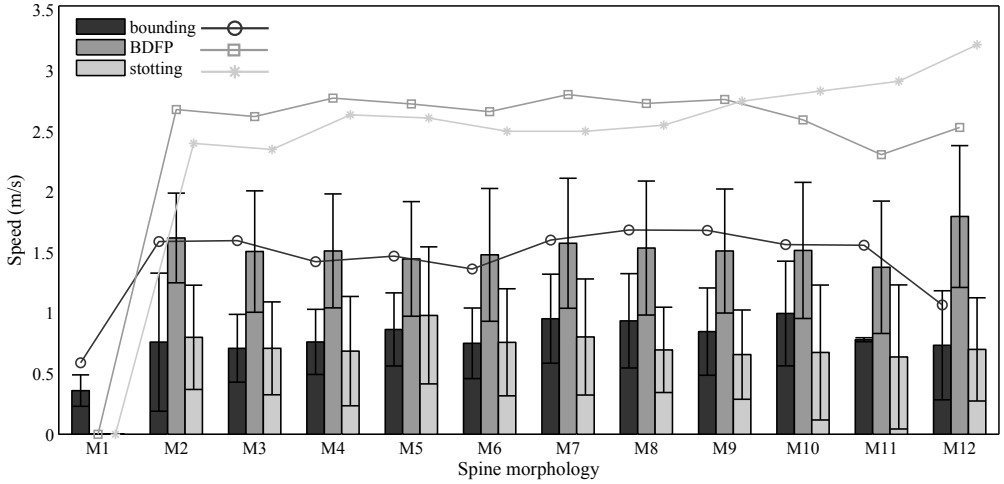

Figure 10. Speed over all spine morphologies. X axis is the spine morphology ranging from one to twelve spinal joints. Y axis denotes speed. The average speed, the standard derivation and the fastest speed of each morphology are represented by bars, error bars, and pointed lines, respectively.

5. Conclusion and Discussion

This novel study has successfully tested the biological concept of "Spinal Engine" and demonstrated spine-driven locomotion in a quadruped robot where legs are not actuated. It suggests that the motion of the spine is a determinant factor in the locomotion, working as an engine to propel the body; limbs might be looked at as servants of the trunk to assist locomotion [7].

$M2$ performs better than $M1$ in terms of the speed and stability. $M2$ is able to produce

more freedom to pull the rear legs forward, increase the stride length, and move the CoM more efficiently forward. Therefore the speed is increased. In addition, it benefits stability by using additional TJ to optimize the movement generated by the LJ by readjusting unstable posture or enhancing the extension-flexion movement.

$I2$ and $I3$ mainly differ in the speed and the gait. $I3$ reaches the maximal extension and flexion in two flight phases per stride, while $I2$ is only suspended once in each stride. In addition, the gait of $I3$ exhibits greater proportion of flight in total stride. These results are in agreement with studies of the motions of the running cheetah and horse [17]. A horse, with relatively rigid spine generating less spinal movements [21], can be represented by $I2$, and a cheetah, featuring pronounced spinal movements, is suitable to be simplified as $I3$. We conclude that the double flight phases, together with greater proportion of flight, contribute to its longer stride [17].

Stotting gait emerges when the spinal flexion-extension is enough high. It exhibits much higher GC and wider vertical excursion of CoM. In addition, the stance phase between spinal flexion and extension phase is missing, which has the function to transfer energy and power the spinal extension movements [23]. We think such features lead to energy inefficiency and slow speed. Therefore it is not a suitable model for fast locomotion. Instead, it plays a role in communication [24], e.g., tell predator that it has been seen, and warn its group members of the danger.

In the experiments of exploring multiple spinal joints, first, we found that the $BDFP$ gait has a faster speed than the bounding and stotting gait over all of the spine morphologies ranging from two to twelve spinal joints. Second, the $BDFP$ gait spreads almost all of the spine morphologies, except $M1$. Moreover, as discussed before, the $BDFP$ gait, which features double flight phases, is able to emulate cheetah-like locomotive behaviours to a great extent. Therefore we believe that $BDFP$ gait is a more biologically inspired locomotive behavior.

The amplitude of the vertical motion relative to the nose is about 13%, 13%, 18% of the body length in $I1$, $I2$, $I3$, respectively (Table 3). This is higher than the average value of 10% observed from human [25] and pika [19] running. The reduction of the vertical displacement of CoM could be achieved by introducing springs in the legs and adjusting their spring-mass systems by increasing the angle swept by the stance legs while keeping leg stiffness nearly constant [26].This will be one of topics in the future. In addition, the way of how to coordinate legs and the spine's movements will be investigated.

More importantly, the introduction of elastic elements to the spine is crucial to get closer to the biological spine model to investigate the energy efficiency, energy transfer, etc. In this case, force control of actuation joint in Matlab simulator will be employed and the methods to tune the force will be studied as well.

If we look back to nature, we find that most of features of the spine are asymmetrical, for example, different length of lumbosacral spine, thoracic spine. In this study, when the number of spinal joints are greater than one, all of the joints in this morphology have possibilities to rotate within certain degrees or stop moving, because of the setting of the motion range. If one joint or some joints choose to stop rotating, then the distribution of rotation spinal joints becomes asymmetrical case. Therefore, our current results are applicable to these asymmetrical cases. However, there still exists a lot of room to study the effect of asymmetrical structures on locomotion, e.g., the unevenly distritbuted spine weights.

Furthermore, a more biologically inspired controller, e.g., central pattern generater, will be taken into account in the future work, with the attempt to better mimic the animals spine locomotive mechanism.

In the near future, on-site experiment is necessary to be implemented to validate the correctness of these optimized gaits. Since the results show that two spinal joints are sufficient to represent a biological spine, we will improve the Kitty robot [12] by adding one additional spinal joint to validate the simulated results.

References

[1] Raibert M. legged robots that balance. The MIT Press. 2000.

[2] Poulakakis I, Smith JA, Buehler M. Modeling and experiments of untethered quadrupedal running with a bounding gait: The scout ii robot. The International Journal of Robotics Research. 2005; 24(4):239–256.

[3] Byl K, Tedrake R. Dynamically diverse legged locomotion for rough terrain. In: 2009 ieee international conference on robotics and automation (icra). 2009 May. p. 1607–1608.

[4] Schilling N, Carrier DR. Function of the epaxial muscles in walking, trotting and galloping dogs: implications for the evolution of epaxial muscle function in tetrapods. The Journal of Experimental Biology. 2010;213(9):1490–1502.

[5] Gracovetsky S. An hypothesis for the role of the spine in human locomotion: a challenge to current thinking. Journal of Biomedical Engineering. 1985;7(3):205–216.

[6] Gracovetsky S, Iacono S. Energy transfers in the spinal engine. Journal of Biomedical Engineering. 1987;9(2):99–114.

[7] Gracovetsky S. The spinal engine. Springer, cop. 1989.

[8] Lewis MA, Bekey GA. Gait adaptation in a quadruped robot. Autonomous Robots. 2002;12:301–312.

[9] Culha U, Saranli U. Quadrupedal bounding with an actuated spinal joint. In: 2011 ieee international conference on robotics and automation (icra). 2011 May. p. 1392–1397.

[10] Pfeifer R, Bongard J. How the body shapes the way we think: A new view of intelligence. The MIT Press. 2006.

[11] Zhao Q, Sumioka H, Pfeifer R. The effect of morphology on the spinal engine driven locomotion in a quadruped robot. In: The 5th international symposium on adaptive motion of animals and machines (amam2011). 2011 Oct. p. 51–52.

[12] Zhao Q, Nakajima K, Sumioka H, Yu X, Pfeifer R. Embodiment enables the spinal engine on quadruped robot locomotion. In: 2012 ieee/rsj internattional conference on intelligent robots and systems. 2012 Oct. p. 2449–2456.

[13] Tsujita K, Kobayashi T, Inoura T, Masuda T. Gait transition by tuning muscle tones using pneumatic actuators in quadruped locomotion. In: 2008 ieee/rsj international conference on intelligent robots and systems (iros). 2008 Sept. p. 2453–2458.

[14] Fischer MS, Witte H. Legs evolved only at the end! Philosophical Transactions of the Royal Society A: Mathematical, Physical and Engineering Sciences. 2007;365(1850):185–198.

[15] Billy. Spinal coord injury resource center. 2012. Available from: http://www.spinalinjury.net/index.html.

[16] Warnecke L. The stem of aplombcpart two: The thoracic spine. 2012. Available from: http://danceadvantage.net/2011/03/09/thoracic-spine/.

[17] Hildebrand M. Motions of the running cheetah and horse. journal of the Royal Society Interface the Royal Society. 1959;40(4):481–495.

[18] Haupt PL, Haupt SE. Practical genetic algorithms (second edition). John Wiley & Sons, Inc.˙2004.

[19] Hackert R, Witte H, Fischer MS. Interactions between motions of the trunk and the angle of attack of the forelimbs in synchronous gaits of the pika (ochotona rufescens). In: Adaptive motion of animals and machines. 2006. p. 69–77.

[20] Macpherson JM, Ye Y. The cat vertebral column: stance configuration and range of motion. Experimental brain research Experimentelle Hirnforschung Expérimentation cérébrale. 1998 Apr; 119(3):324–32.

[21] Townsend HG, Leach DH, Fretz PB. Kinematics of the equine thoracolumbar spine. Equine veterinary journal. 1983 Apr;15(2):117–22.

[22] Schilling N, Hackert R. Sagittal spine movements of small therian mammals during asymmetrical gaits. The Journal of Experimental Biology. 2006;209:3925–3939.

[23] Alexander RM. Why mammals gallop. American Zoologist. 1988;28(1):237–245.

[24] Caro T. The functions of stotting in thomson's gazelles: some tests of the predictions. Animal Behaviour. 1986;34(3):663 – 684.

[25] Lee CR, Farley CT. Determinants of the center of mass trajectory in human walking and running. Journal of Experimental Biology. 1998;201(21):2935–44.

[26] Farley CT, Glasheen J, McMahon TA. Running springs: speed and animal size. Journal of Experimental Biology. 1993;185(1):71–86.